Published by :
http://www.ijert.org

International Journal of Engineering Research & Technology (IJERT)
ISSN: 2278-0181
Vol. 8 Issue 11, November-2019

Dynamic Analysis and Intelligent Electro-Dynamic Control of Aero-Engine Rotor-Bearing System

Y. Hari Krishna, T. Pavan Kumar, M. Sridhar, Y. Bhavana, C. Sai Surya Bhagavan
Andhra University
Andhra Pradesh.

Abstract. **In the present work, dynamic analysis of a typical two-spool aero-engine turbo-compressor rotor system mounted on ball bearings supported with squeeze-film dampers is considered. The dynamic equations are established by the finite element model and the reduced assembled system of equations are solved to obtain transient unbalance response and frequency domain plots during startup (acceleration) conditions. The nonlinear bearing forces with squeeze-film damper loads at the rotor nodes are considered during analysis. An electromagnetic actuator is employed based on a trained neural network data for amplitude control at the specific location on the rotor. Unlike, the conventional PD-control scheme, proposed controller can predict the required component forces based on the instantaneous radial displacements at that location. Interactive computer programs are developed to simulate the practical system by considering various forces including gyroscopic, gravity in addition to nonlinear bearing forces.**

Keywords: Transient analysis, Beam elements, Electrodynamic actuator, Neural network observer, Two-spool engine.

1 INTRODUCTION

Now-a-days, rotor models have become more and more complex due to increasing demands of engineering applications. The simplified nonlinear dynamic models of rotors cannot reflect the practical conditions. Therefore, more complex, flexible rotor-bearing models such as those using one-dimensional Timoshenko beam elements, transfer matrix methods and mode synthesis techniques are needed. Most recent aspect is to control the critical response amplitudes in an online fashion. In this line, various strategies [1-3] have been proposed in literature to increase the damping such as semi-active magneto-rheological fluids, electromagnetic bearings and visco-elastic supports. In practice, augmentation of damping is a difficult task and alternatively active control techniques became the choice. The active control capability to stabilize rotors and reduce unbalance vibration was illustrated in literature by several authors [4-8]. These works do not consider the time-varying plant dynamics, so that the robustness of controller may not be guaranteed. Robust stability issues were later-on shown by few other papers [9-11]. It was proved that the model identification and control as integral aspects in the robust controller design.

Recently, the active vibration control of rotors using electromagnetic exciters is one of the important topics in the turbomachinery analysis. Control of resonance amplitudes and reduction of local vibration levels is possible on-line with electromagnetic coils. In [12-13] and [14-16], illustrated the local control approach using linear PD control technique for high-speed rotors mounted on hydrodynamic and rolling element bearings. A hybrid approach of intelligent PID feedback control to suppress vibrations in the critical zones presented [17]. An attenuating method [18] for lateral vibration of rotors with the aid of semi-active dampers and active control of hydrodynamic bearings illustrated. In [19] used primary optimal control gain of genetic algorithm in proportional derivative control to get stability in the rotor system. A nonlinear golden section adaptive control algorithm to reduce the vibration levels of a flexible Cartesian smart material manipulator run by a servomotor implemented [20]. In [21] employed two piezoactuators to actuate two movable bushing to control the rotor at high speeds. The output error signal coming from the proximity probe is responsible to control the piezoactuator acting force at the bushings. The change of the magnetic flux induced in the electric coils is responsible for the controlling damping effect of the dampers. An adaptive control approach [22] proposed to suppress vibrations due to imbalance of masses in the rotors and [23] proposed a method to convert the complex domain modes of a rigid rotor supported on active magnetic bearings to achieve maximum PID control performance in the system. Most of the control schemes proposed in rotors are based on linear concepts. To augment the controller performance in nonlinear rotor systems, an attempt is required to design and test a real time strategy by using some inverse approach.

In the present work, a typical two-spool aero-engine turbo-compressor rotor system supported by ball bearings is considered. The nonlinear dynamic equations are solved using time-integration scheme and the transient response stability issues are discussed during acceleration/deceleration condition. An electromagnetic actuator design based on a trained neural network is implemented for controlling the vibration amplitudes at a specific location of the rotor. Dynamic analysis and control simulations are illustrated at different speeds of operation. Remainder of the paper is organized as follows: section-2 presents the modeling of rotor bearing system with squeeze-film damper force considerations. Section-3 gives the mathematical concept of electromagnetic actuator and its control schemes. Section-4 outlines the results using a numerical example.

International Journal of Engineering Research & Technology (IJERT)
ISSN: 2278-0181
Vol. 8 Issue 11, November-2019

2 MATHEMATICAL MODELING

Modern aero-engine rotors have multi-spool configurations [24-30] due to their several advantages. In multi-spool engine rotors, as the air flows through the compressor, it's pressure and temperature rises, increasing the speed. Two or more concentric shafts operating at different speeds are commonly used. Each spool is given by a separate turbine stage and runs at different speeds. A two-spool engine rotor considered in the present work with flexible bearings is shown in Fig. 1.

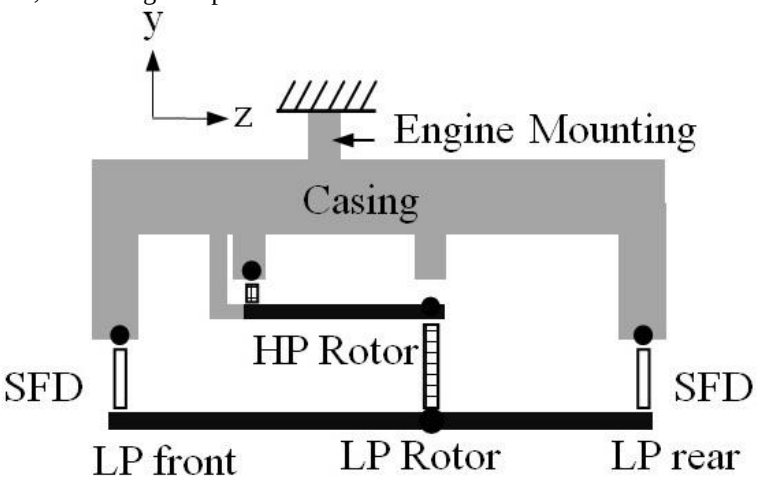

Fig. 1. Schematic diagram of a two-spool engine

The assembly of whole structure is consisting of high pressure (LP) turbine and low pressure (LP) compressor. Four bearings with a casing are used to support the entire structure. The HP shaft on the front end is having the casing to support the SFD bearing through a squirrel case spring and this will provide the actual axial location of parallelism of the HP rotor in the oil annulus. The dynamic analysis of this rotor system is carried out using a finite element model. Two-node 8-degrees of freedom Timoshenko beam elements are used to discretize the assembly. It is assumed that the torsional and axial deformations are negligible. Fig. 2 shows the simplified model of the twin-spool rotor assembly.

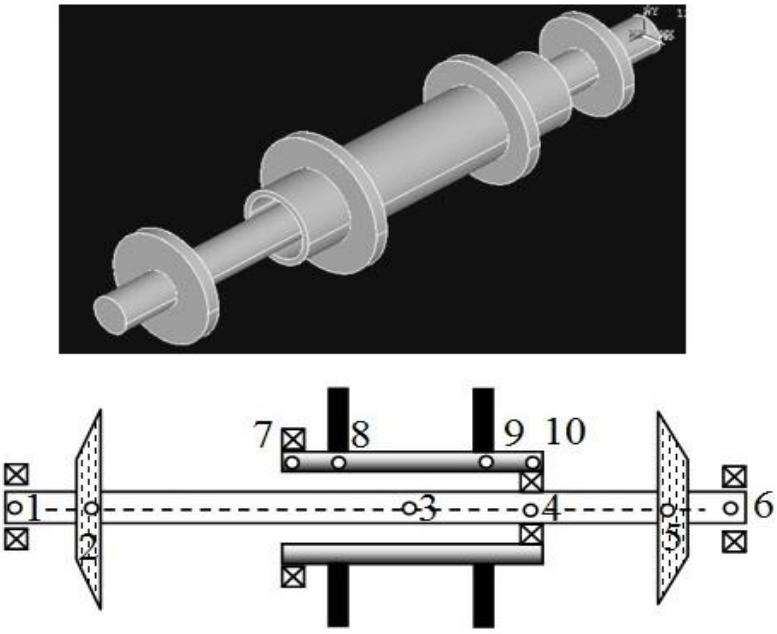

Fig. 2. The FE model of LP and HP rotor system.

It consists of four bearings and four disks, two each on inner and outer spools respectively. It is considered that the unbalance acts on all the four disks and bearings are rolling element bearings supported in squeeze-film dampers. The simplified configuration is different from the conventional model in consideration of nonlinear bearing forces as compared to conventional spring-damper bearing elements. As seen in the figure, the node 4 of inner spool and node 10 of outer spool is connected by the fourth bearing element.

International Journal of Engineering Research & Technology (IJERT)
ISSN: 2278-0181
Vol. 8 Issue 11, November-2019

2.1 Equations of motion

By considering rigid disc, flexible shaft model, the rotor-bearing system is discretized into eight beam elements along with four lumped disk masses. Bearing and unbalance forces are accounted as external force vector. By using energy expressions and applying the Hamilton principle, the governing equation of motion for the system are given by

$$[M]\{\ddot{q}\} + ([C] + (\omega_0 + \alpha t)[G])\{\dot{q}\} + [K]\{q\} = \{F_e\} + \{F_b\} + \{F_s\} + \{F_g\} \quad (1)$$

Where $[C]$, $[G]$ are the viscous and gyroscopic damping matrices. $[K]$ and $[M]$ are the assembled stiffness and assembled mass matrices, $\{F_e\}$ is the unbalance force vector, $\{F_b\}$ bearing force vector, $\{F_s\}$ is the squeeze film force vector, $\{F_g\}$ is the gravity force vector and $\{q\}$ is the vector of nodal displacements. Also, ω_0 is initial velocity, t is the time and α is constant acceleration. Altogether five elements (6×4=24 degrees of freedom) are taken on inner spool and three elements (4×4=16 degrees of freedom) are on the outer spool.

2.2 Squeeze-Film Damper Bearing

The main advantage of Squeeze film dampers is to attenuate the unbalance synchronous response of a rotor and to unbalance and to reduce sub-synchronous rotor dynamic instabilities. The required external damping for the roller element bearings used in Aircraft engines are provided with one or more SFDs to support the rotor. Normally, a lubricating film is provided in between a whirling journal and a stationary housing. The typical rolling element bearing outer race is constrained with a squirrel cage or a dowel pin (elastic) support to arrest the rotation along with the journal. Pressurized lubricant fills the squeeze film lands through the central groove or feed holes. The squeeze oil film will be pressurized due to the rotation of the inner race with the rotor and the outer race will be in stationary position within the housing. Due to the lubricant fluid film reaction forces, dynamic pressure will be generated and that will support to damp the increase rotor whirl motion amplitudes.

Lubricant viscosity, journal kinematics and damper geometry are the important factor in controlling the force generated due to fluid film reaction in a SFD bearing. Fig.3 shows the schematic of SFD bearings.

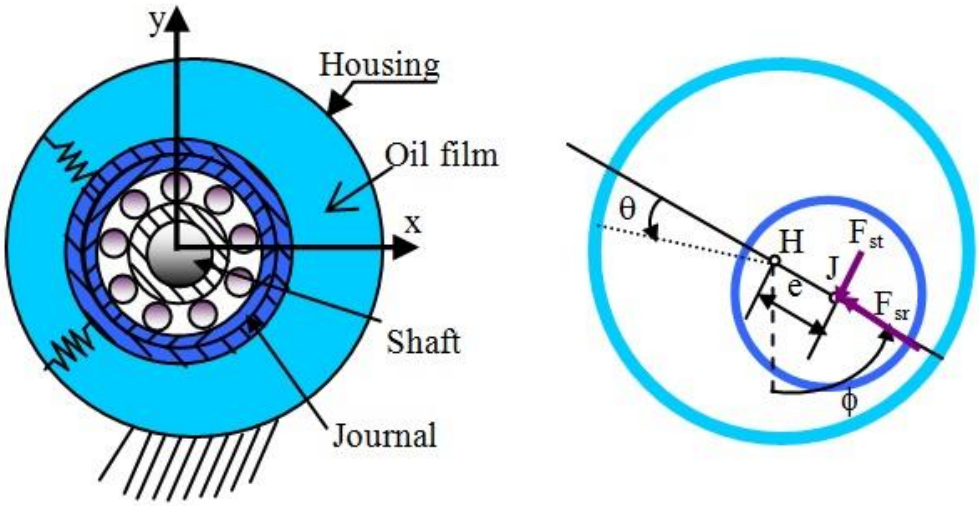

Fig. 3. Schematic of SFD bearing system.

Here, the outer race (journal) is connected to the casing through a centralizing spring. The bearing forces are due to contact between the balls and races, which are obtained using the following Hertz contact force relations [31]:

$$F_{bx} = -\sum_{j=1}^{N_b} K_b\left(x\cos\theta_j + y\sin\theta_j - r_0\right)^{3/2} H.\cos\theta_j \quad (2a)$$

$$F_{by} = -\sum_{j=1}^{N_b} K_b\left(x\cos\theta_j + y\sin\theta_j - r_0\right)^{3/2} H.\sin\theta_j \quad (2b)$$

where r_0, K_b and H are the radial clearance, Heaviside function and the Hertz contact stiffness and is depends on the contact material and shape, respectively. x & y are the coordinates. The jth ball angular location term θ_j can be written as

$$\theta_j = \omega_{Cage} \times t + \frac{2\pi}{N_b}(j-1);\ j=1,2,\ldots N_b \quad (3)$$

where ω_{Cage} is the ball bearing cage angular velocity is written as $\omega_{Cage}=\omega\times r/(R+r)$ with R and r as the radii of the outer and inner races and ω is the rotational speed of shaft, N_b is balls number. The ball passing frequency or Variable Compliance (VC) is defined as $\omega_{VC}=\omega_{Cage}\times$ Number of balls (N_b). It is assumed that outer race rotates about its axis, but does not spin in the oil film. The relative displacement between the shaft (s) and outer race (o) is given by, $x= x_s-x_o$, $y=y_s-y_o$. The outer race (journal) is subjected to squeeze-film oil forces. The solution of the Reynolds equation for incompressible fluids written below will give the instantaneous pressure distribution p inside the oil film [32]:

International Journal of Engineering Research & Technology (IJERT)
ISSN: 2278-0181
Vol. 8 Issue 11, November-2019

$$\frac{1}{R_1^2}\frac{\partial}{\partial\theta}\left\{h^3\left(\frac{\partial p}{\partial\theta}\right)\right\}+h^3\frac{\partial^2 p}{\partial z^2}=12\mu\left(e\dot{\phi}\sin\theta+\dot{e}\cos\theta\right) \quad (4)$$

Here, h= c+ecosθ is called squeeze-film thickness.
The simplified force components of oil film in the x-y stationary coordinate system can be obtained from the following important assumptions:
(i) Oil-film thickness when compared to radius of journal is small, (ii) pressure gradient along the radial direction is small and (iii) laminar lubricant fluid flow.
The resulting squeeze-film forces are given from the pressure distribution as:

$$F_{sx}=-\frac{\pi R_1 L^3}{c^2}\left[\left(\dot{\varepsilon}\,I_1+\varepsilon\dot{\phi}\,I_2\right)\cos\phi-\left(\dot{\varepsilon}\,I_2+\varepsilon\dot{\phi}\,I_3\right)\sin\phi\right] \quad (5a)$$

$$F_{sy}=-\frac{\pi R_1 L^3}{c^2}\left[\left(\dot{\varepsilon}\,I_1+\varepsilon\dot{\phi}\,I_2\right)\sin\phi-\left(\dot{\varepsilon}\,I_2+\varepsilon\dot{\phi}\,I_3\right)\cos\phi\right] \quad (5b)$$

where R_1, μ, c and L are the radius of SFD, oil dynamic viscosity, the radial clearance of squeeze film damper and the land length of squeeze film damper respectively. The eccentricity ratio ε is given by: $\varepsilon=\frac{\sqrt{X^2+Y^2}}{c}$. $\phi=\tan^{-1}(Y/X)$. $\dot{\phi}$ is the angular velocity of SFD and (X,Y) is the displacement of SFD in the fixed coordinate system and I_1, I_2 and I_3 are the bearing integrals and evaluated analytically in closed form and given by [33]:

$$I_1=\int_{\theta_1}^{\theta_1+\pi}\frac{\cos^2\theta}{(1+\varepsilon\cos\theta)^3}d\theta \quad (6a)$$

$$I_2=\int_{\theta_1}^{\theta_1+\pi}\frac{\sin\theta\cos\theta}{(1+\varepsilon\cos\theta)^3}d\theta \quad (6b)$$

$$I_3=\int_{\theta_1}^{\theta_1+\pi}\frac{\sin^2\theta}{(1+\varepsilon\cos\theta)^3}d\theta \quad (6c)$$

$$\theta_1=\tan^{-1}\left(-\frac{\dot{\varepsilon}}{\varepsilon\dot{\phi}}\right) \quad (6d)$$

All these forces are incorporated in Eq.(1) at appropriate nodes and the resultant equations are solved. In present case, these squeeze-film damper forces are considered only on LP rotor front and rear bearings.

3 ELECTROMAGNETIC ACTUATOR MODEL

The electromagnetic actuator with four- pole is shown in the Fig. 4. Poles 1 and 2 provide actuation force in vertical (x) direction and poles 3 and 4 provide actuation force in the horizontal (y) direction.

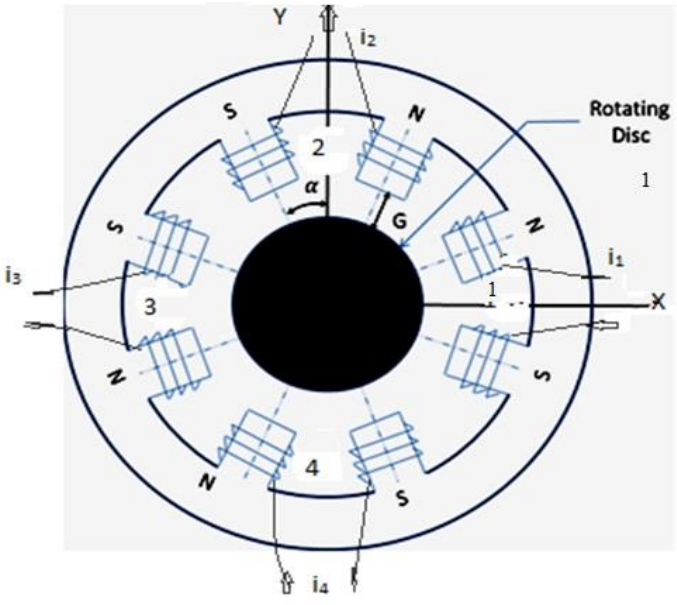

Fig. 4. Four-pole electromagnetic actuator.

The expressions for actuation force in vertical and horizontal direction are:

$$F_{ax}=F_{ax1}-F_{ax3}=\mu_0 A_a N^2\cos\alpha\left[\frac{(I_b+i_1)^2}{(G-x\cos\alpha)^2}-\frac{(I_b+i_3)^2}{(G+x\cos\alpha)^2}\right] \quad (7a)$$

$$F_{ay}=F_{ay2}-F_{ay4}=\mu_0 A_a N^2\cos\alpha\left[\frac{(I_b+i_2)^2}{(G-y\cos\alpha)^2}-\frac{(I_b+i_4)^2}{(G+y\cos\alpha)^2}\right] \quad (7b)$$

International Journal of Engineering Research & Technology (IJERT)
ISSN: 2278-0181
Vol. 8 Issue 11, November-2019

Where μ_0 is permeability of free-space ($\mu_0 = 4 \times 10^{-7}$H/m), A_a is the cross-section of the air-gap which is assumed to be equal to pole face area, N is the number of turns per pole, G is a nominal air gap between stator and rotor, α is half the included angle of a pole (α =22.5°), I_b is bias current which is kept fixed and i_n (n = 1, 2, 3 and 4) are small variable current of corresponding poles which are varied according to control strategy. For the sake of simplicity currents in the diametrically opposite poles are kept equal in magnitude, but opposite in direction, i.e., $i_1 = -i_3$ and $i_2 = -i_4$. In the actuator design, the allowable displacement of the rotor is considered about one-tenth of the air gap size. At normal point of operation, $i_1=i_2=i_3=i_4=0$ and x=y=0. By expanding with Taylor series and neglecting higher order terms, we get:

$$F_{ax} = \frac{4\mu_0 A_g N^2 I_b cos\alpha}{G^2} i_1 + \frac{4\mu_0 A_g N^2 I_b{}^2 cos^2\alpha}{G^3} x = k_{1a} i_1 + k_{2a} x \quad (8a)$$

$$F_{ay} = \frac{4\mu_0 A_g N^2 I_b cos\alpha}{G^2} i_2 + \frac{4\mu_0 A_g N^2 I_b{}^2 cos^2\alpha}{G^3} y = k_{1a} i_2 + k_{2a} y \quad (8b)$$

Here, k_{1a} and k_{2a} are force-current and force-displacement constants of electromagnetic actuator respectively. Computation of currents i_1 and i_2 as a function of instantaneous errors is the function of controller.

3.1 Design of PD Controller

To minimize the vibration amplitude of system appropriate magnetic force should applied by the actuator; force should act in the opposite direction of motion and should increase with displacement. As seen from above simplified equations, the magnetic force depends upon the pole winding current of an electromagnet; so by controlling pole winding currents, the system response can be controlled. Proportional-Derivative (PD) control is generally used for faster response. Proportional control increase the control input in proportion to the error e(t) within the acceptable range of error. Derivative control changes the control input in proportion to rate of change of error $\dot{e}$. Equation of control output of PD controller using proportional and derivative gains K_p, K_d can be given as

$$u(t) = K_p e(t) + K_d \dot{e}(t) \quad (9)$$

The controlled output is currents and the error signal. Hence, the control currents for pole pair in horizontal direction (i_1) and in the vertical direction (i_2) are given as [12]:

$$i_1 = K_p e_x(t) + K_d \dot{e}_x(t) \quad (10\,a)$$

$$i_2 = K_p e_y(t) + K_d \dot{e}_y(t) \quad (10\,b)$$

As the set point is having zero velocity and displacement, the terms $e_x(t) = -x$ and $e_y(t) = -y$ along with $\dot{e}_x(t) = -\dot{x}$ and $\dot{e}_y(t) = -\dot{y}$. Designer has to select the appropriate gain constants K_p and K_d and obtain the control forces F_{ax} and F_{ay}.

3.2 Neural network based controller

As seen from Eq.(7), it is observed that the control forces are functions of the velocities of rotor and its radial displacements. The control function in non linear in nature. So, a control concept similar to an inverse dynamic model of the system is used. A nonlinear controller based on trained neural network model with instantaneous transient response as inputs and corresponding currents as outputs is proposed in present work. Fig.5 shows the block diagram of the control methodology.

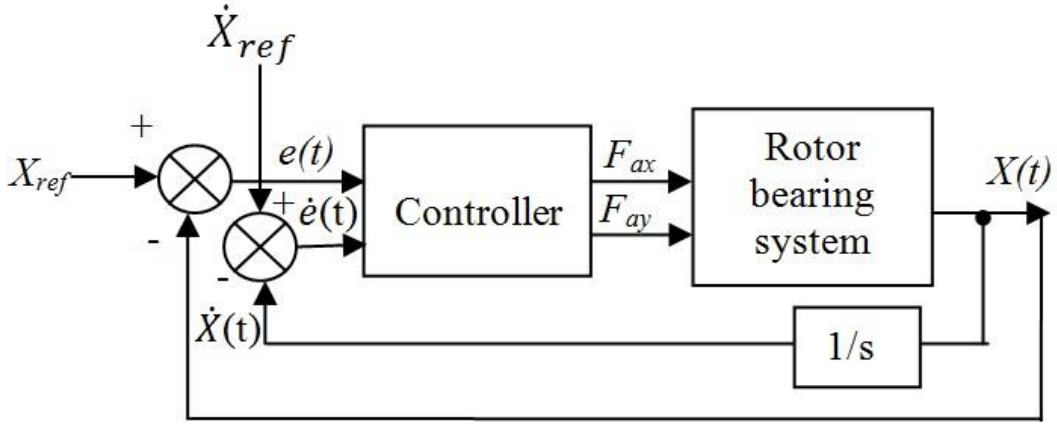

Fig. 5. Error based control scheme.

Conventional 3-layer back propagation neural network is used to train the data. The inputs for the neural network are errors (vector of negative X(t) values) and error rates (vector of negative $\dot{X}(t)$ values) over a sampling period as the values of i_1 and i_2 are varied randomly from 0 to 100 milli-amperes according to equations (7). A 4 input (*-x*, *-y*, *-ẋ* and *-ẏ*) and two output (i_1, i_2) training patterns generated inversely have been used in training. Learning rate of 0.4 and momentum

International Journal of Engineering Research & Technology (IJERT)
ISSN: 2278-0181
Vol. 8 Issue 11, November-2019

factor of 0.01 are implemented. Optimum hidden layer nodes were found to be 4 and the neural network is trained using an interactive computer program to find the set of weight matrices. Further, these are employed in estimating the unknown currents corresponding to a computed nodal displacement and velocity vectors during every time step. The detailed backpropagation algorithm for 3-layer multilayer perceptron network can be found in open literature [34].

4 RESULTS AND DISCUSSIONS

The coupled set of differential equations is evaluated in time-domain series with aid of Runge-Kutta equation of order four with initial value as zero. The dimensional properties of the rotor used in the analysis shown in Table 1. A speed ratio of 1.5 is implemented between HP and LP rotors. The material for the spools is steel with modulus of elasticity value E=210 GPa and density ρ=7.8 g/cm^3. All four disks have polar moment of inertia (I_P) twice the diametric mass moment of inertia (I_D). Further, an eccentricity of 10 microns is considered in the disks. The resultant stiffness, mass, damping (damping factor of 0.01) and gyroscopic matrices are used. The SFD parameters used are [35]: $\mu=5\times10^{-3}$ PaS, $c=2\times10^{-4}$ m, $L=8.3\times10^{-3}$ m, R_1=0.03 m. The value of ω is set as 2000 rpm and angular acceleration α is varied.

Table I Geometric and material data for rotor (Referring to Fig.2)

Node	Axial dist.(mm)	d_{outer} (mm)	d_{inner} (mm)	Disc mass(kg)	I_P (kg-mm^2)
1	0	30.4	0	-	-
2	76.2	30.4	0	4.904	0.02712
3	323.85	30.4	0	-	-
4	406.4	30.4	0	-	-
5	457.2	30.4	0	4.203	0.02034
6	508	30.4	0	-	-
7	152.4	50.8	38.1	-	-
8	203.2	50.8	38.1	3.327	0.01469
9	355.6	50.8	38.1	2.227	0.0972
10	406.4	50.8	38.1	-	-

Fig.6 depicts the frequency response plot of a system considering ball bearing forces and not considering the forces. Fig.6(a) coincides well with the available results. It is seen that there are multiple ball passing frequencies (VC) along with harmonics in the system, when ball bearing forces are accounted.

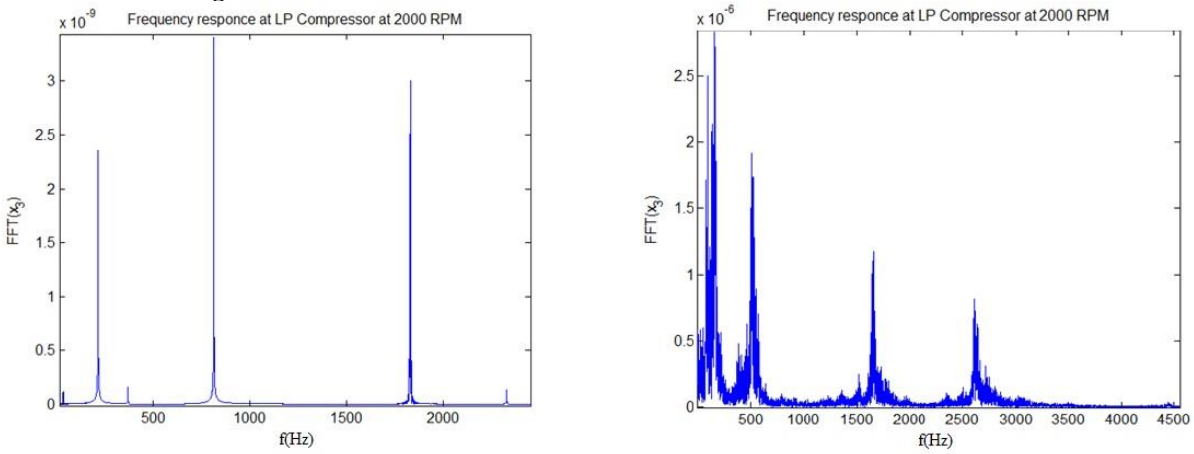

(a) Bearings as spring-damper system (b) Bearings with forces considered

Fig. 6. Frequency plots of rotor at speed of 2000 rpm.

Fig.7 shows the transient analysis results at different acceleration conditions in terms of frequency responses. It is obvious that the multiplicities of ball passing frequencies increase with acceleration of rotor. This may be due to a randomly changing bearing excitation.

International Journal of Engineering Research & Technology (IJERT)
ISSN: 2278-0181
Vol. 8 Issue 11, November-2019

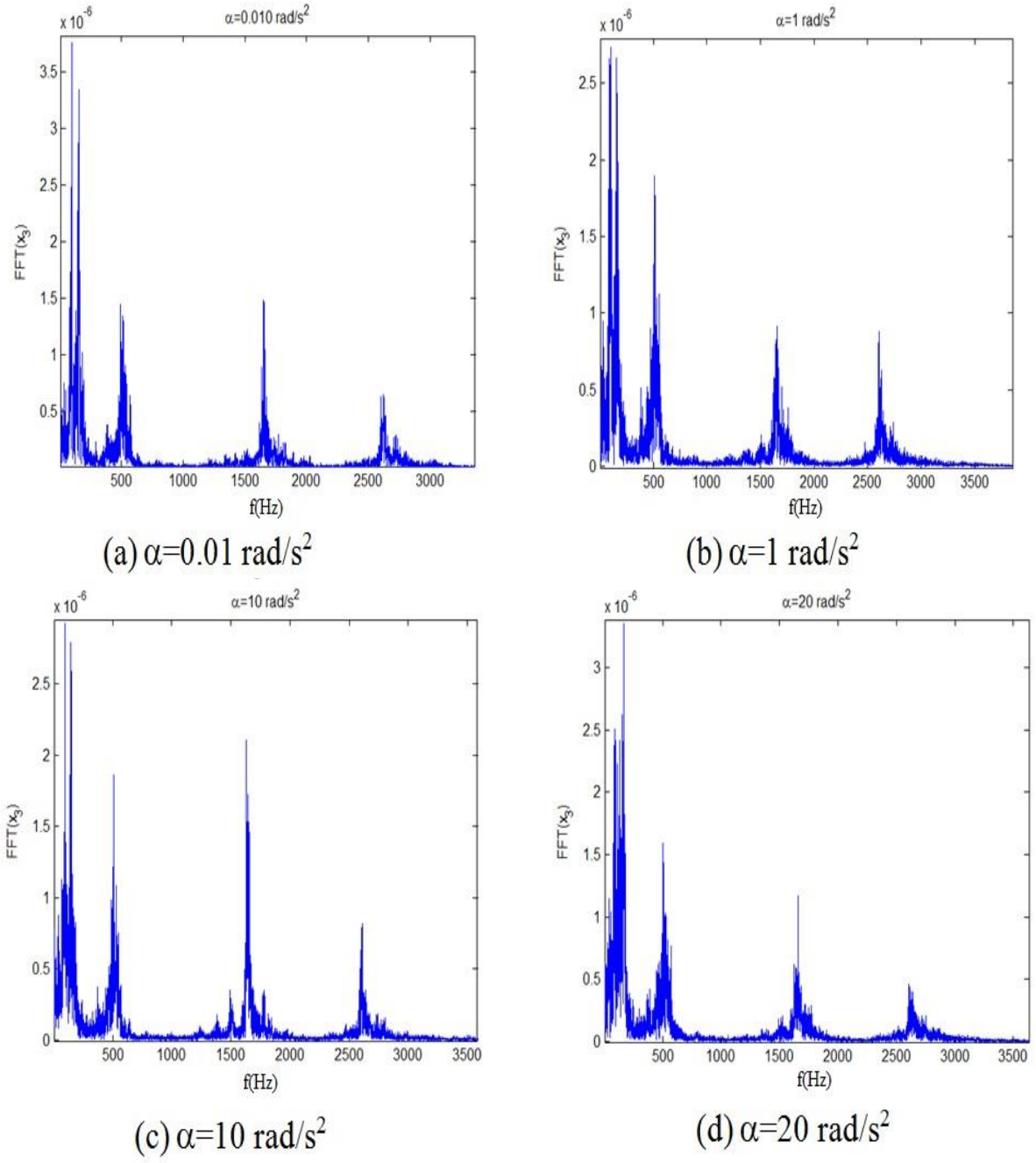

Fig. 7. Effect of acceleration of rotor at LP compressor disk.

In order to minimize the amplitude levels, the following electromagnetic actuator parameters are considered: N=106, G=9 cm ,A_g=2.4 cm^2, α=22.5°, and I_b=3 A. The instantaneous current components i_1 and i_2 depend on the displacements x and y at the disk node-1. The software code is modified to incorporate an extra component of magnetic force on the force vector at right side located at disk-1 Fig.8 shows the frequency response plots of rotor computed when controlled with bearing force and when uncontrolled with force. It indicates that the amplitudes from second mode have reduced drastically and the ball passing frequency amplitudes have been dropped. The methodology can be extended for other nodes of interest.

International Journal of Engineering Research & Technology (IJERT)
ISSN: 2278-0181
Vol. 8 Issue 11, November-2019

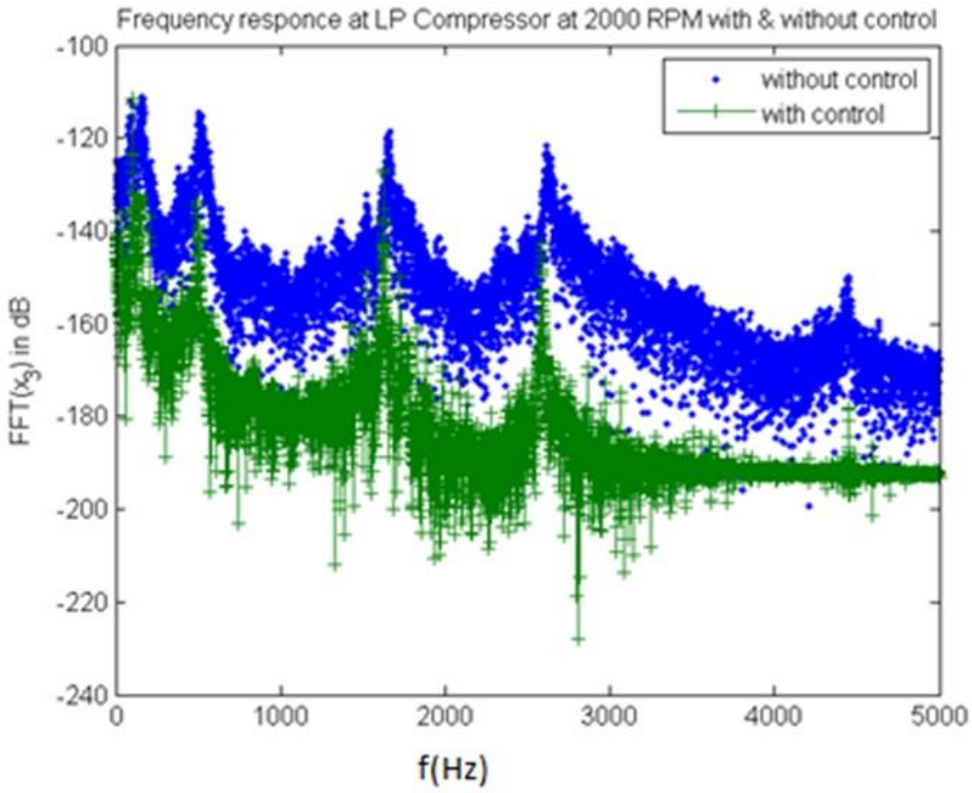

Fig. 8. Amplitude reduction at disk-1 node with EM controller.

5 CONCLUSIONS

In current study, a process to reduce vibration with electromagnetic actuators has been briefly presented for a twin-spool rotor case study. The considered system has unbalance and gravity loading along under accelerating conditions. Gyroscopic effects arising due to combined effect of the shaft and disks were accounted, and for all disks unbalance was taken into consideration. Frequency response diagrams were used to distinguish the dynamic response at different angular accelerations of the rotor. It was observed that the squeeze-film damper at the front and rear ends of LP rotor have drastically reduced the amplitudes at critical speeds of operation. Further, the neural-network based electromagnetic actuator designed to provide the nonlinear control forces has considerably reduced the response. Unlike the conventional PD control scheme, the present approach, do not search for optimum set of controller gains. However, it requires huge set of input-output training data before its implementation in the plant. Although the results were illustrated for a selected speed of LP rotor, the focus may be given at the critical speeds of operation in practice so as to identify the effective operational speed range for amplitude attenuation using EM actuator.

REFERENCES

[1] Zhu C, A disk-type magneto-rheological fluid damper for rotor system vibration control. J Sou Vib 2005;283:1051-1069.
[2] Fan YH, Lee AC. Design of a permanent/electromagnetic magnetic bearing- controlled rotor system. J Fran Inst 1997;334:337-356.
[3] Verichev NN, Verichev SN, Erofeyev VI. Damping lateral vibrations in rotary machinery using motor speed modulation. J Sou Vib 2010;329:13-20.
[4] Zhong J, Li L. Fractional-order system identification and proportional-derivative control of a solid-core magnetic bearing. ISA Trans 2013;
[5] Burrows C, Sahinkaya M, Clements S. Active vibration control of flexible rotors: an experimental and theoretical study. Proc Roy Soc Lon A 1989;422:123-146.
[6] Lin YH, Yu HC. Active modal control of flexible rotor. Mechanical Systems and Signal Processing 2004;18:1117-1131.
[7] Jang MJ, Chen CL, Tsao YM. Sliding mode control for active magnetic bearing system with flexible rotor. J Fran Inst 2005; 342:401-419.
[8] Dimitri A, El-Shafei A. Instability control and unbalance compensation of flexible rotors supported on journal bearings using magnetic bearings. Proceedings of the Eighth IFToMM International Conference on Rotor Dynamics, Seoul, Korea; Sep, 2006. p. 657-664.
[9] Fittro R, Knospe C. Rotor compliance minimization via μ-control of active magnetic bearings. IEEE Trans Con Sys Tech 2002;10(2):238–249.
[10] Riemann B, Perini EA, Cavalca KL, De Castro HF, Rinderknecht S. Oil whip instability control using μ-synthesis technique on a magnetic actuator. J Sou Vib 2013;332:654-673.
[11] Xiaochun G, Dengqing C. Fuzzy proportional-integral-derivative control of an overhang rotor with double discs based on the active tilting pad journal bearing. J Vib Con 2015;19(10):1487-1498.
[12] Fan CC, Pan MC. Active elimination of oil and dry whip in a rotating machine with an electromagnetic actuator. Int J Mech Sci 2011:53:126-134.
[13] Fan CC, Pan MC. Experimental study on the whip elimination of rotor-bearing systems with electromagnetic exciters. Mechanism Machine theo 2011;46:290-304.
[14] Das AS, Nighil MC, Dutt JK, Irretier H. Vibration control and stability analysis of rotor-shaft systems with electromagnetic exciters. Mechanism Machine theo 2008;43:1295-1316.
[15] Das AS, Dutt JK, Ray K. Active vibration control of unbalanced flexible rotor- shaft systems parametrically excited due to base motion. Appli Math Mod 2010; 34:2353-2369.
[16] Das AS, Dutt JK, Ray K. Active control of coupled flexible-torsional vibration in a flexible rotor-bearing system using electromagnetic actuator. Int J Nonli Mechan 2011;46:1093-1109.

International Journal of Engineering Research & Technology (IJERT)
ISSN: 2278-0181
Vol. 8 Issue 11, November-2019

[17] Toha SF, Tokhi MO. A Hybrid Control Scheme for a Twin Rotor System with Multi Objective Genetic Algorithm. 12th International Conference on Computer Modelling and Simulation, Emmanuel College Cambridge, United Kingdom; Mar, 2010. p. 20-28.
[18] Ferfecki P, Zapomel J. Investigation of vibration mitigation of flexibly support rigid rotors equipped with controlled elements. Proc Eng 2012; 48:135-142.
[19] Lin J, Zheng YB. Vibration suppression control of smart piezoelectric rotating truss structure by parallel neuro-fuzzy control with genetic algorithm tuning. J Sou Vib 2012;331:3677–3694.
[20] Qiu ZC. Adaptive nonlinear vibration control of a Cartesian flexible manipulator driven by a ballscrew mechanism. Mech Sys Sig Proc 2012;30:248-266.
[21] Tuma J, Simek J, Skuta J, Los J. Active vibration control of journal bearings with the use of piezoactuators. Mech Sys Sig Proc 2013;36:618–629.
[22] Fang J, Xu X, Tang X, Liu H. Adaptive complete suppression of imbalance vibration in AMB systems using gain phase modifier. J Sou Vib 2013;332:6203-6215.
[23] Han WJ, Chong WL. Proportional-integral-derivative control of rigid rotor-active magnetic bearing system via eigenvalue assignment for decoupled translational and conical modes. J Vib Con 2015; 21(12):2372-2393.
[24] Gunter EJ, Li DF, Barrett LE. Unbalance response of a two spool gas turbine engine with squeeze film bearings. ASME Gas turbine conference and products show, Houston, Texas; Mar, 1981.
[25] Shanmugam A, Padmanabhan C. A fixed–free interface component mode synthesis method for rotordynamic analysis. J Sou Vib 2006; 297:664–679.
[26] Sun G, Palazzolo A, Provenza A, Lawrence C, Carney K. Long duration blade loss simulations, including thermal growths for dual-rotor gas turbine engine. J Sou Vib 2008; 316:147-163.
[27] Hai PM, Bonello P. A computational parametric analysis of the vibration of a three-spool aero-engine under multi-frequency unbalance excitation. J Eng Gas Turb Pow 2011;133:072504-1.
[28] Hai PM, Bonello P. A computational parametric analysis of the vibration of a three-spool aero-engine under multifrequency unbalance excitation. Journal of Engineering for Gas Turbines and Power 2011; 133:072504-1-9.
[29] Lin FJ, Chen SY, Huang MS. Adaptive complementary sliding-mode control for thrust active magnetic bearing system. Con Eng Prac 2011; 19:711-722.
[30] Groves KH, Bonello P, Hai PM. Efficient dynamic analysis of a whole aero engine using identified nonlinear bearing models. Proc Inst Mech Eng, Part C: J Mech Eng Sci 2012;226:66-81.
[31] Chen G. Study of nonlinear dynamic response of an unbalanced rotor supported on ball bearing. J Vib Acou, Trans. ASME 2009;131:061001-1-9.
[32] Inayat HJI, Kanki H, Mureithi NW. On the bifurcations of a rigid rotor response in squeeze-film dampers. J Flui Struc 2003;17:433-439.
[33] Liang MA, JunHong Z, Jiew-Wei L, Jun W, Xin L. Dynamic characteristic analysis of a misaligned rotor-bearing system with squeeze-film dampers. J Zhej Univer-Sci 2016;17:614-631.
[34] Freeman JA, Skapura BM. Neural networks: Algorithms, Applications and Programming Techniques, Addison-Wesley, NY. 1990.
[35] Groves KH, Bonello P. Empirical identification of SFD bearings using neural networks. Mech Sys Sig Proc 2013;35:307-323.